海洋化学学術賞（石橋賞）受賞記念論文

Factors controlling the distribution of elements in the ocean

Yuan-Hui Li*

1. Introduction

The dissolved elements in seawater are usually defined as the elements passing through a 0.45μm pore-size filter. The major sources of the dissolved elements in the ocean are rivers and solvable fraction of continental aerosol dusts. Additional sources are fluxes from bottom sediments through diffusion, re-suspension of sediments, and mid-ocean ridge hydrothermal vents. The inputs of dissolved elements from various sources are redistributed within the ocean through the water mass circulation and mixing, biological uptake at surface and release at depth, and are eventually removed to bottom sediments by settling particles through adsorption/desorption processes. Figure 1 represents a simple four-box conveyor belt model of the ocean (Li, 2000). The symbol w is the advection flux of water from the northern surface Atlantic to the deep Atlantic, which flows to the deep Pacific and eventually upwells back to the surface ocean. The w_m represents the water exchange or mixing rate between the surface and deep Atlantic waters; C_0 and C are respectively the concentrations of a given element in the surface and deep Atlantic waters; I, I_b, and I_s are respectively the input flux from rivers and solvable fraction of aerosols to the surface Atlantic, the internal biological flux from the surface to the deep Atlantic, and the output flux from the deep Atlantic to sediments by settling particles. Symbols with asterisks are corresponding parameters for the Pacific Ocean. Whitfield and Turner (1987) classified the elements into conservative, nutrient, scavenged, and mixed types according to the relative magnitude of C_0, C, C_0*, and C*. For the conservative type elements (by definition, $C_0 = C = C_0^* = C^*$), the

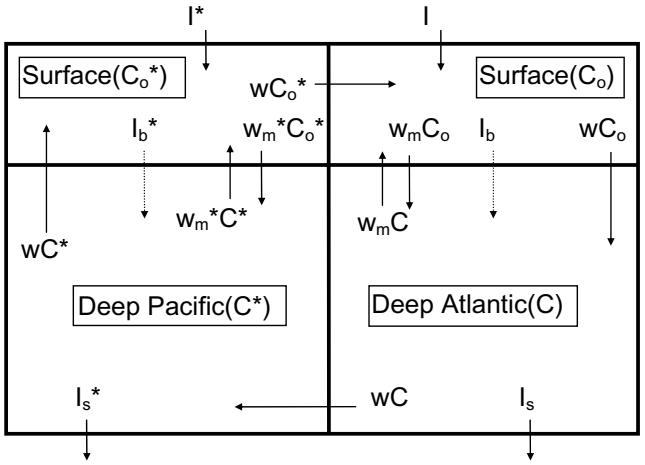

Figure 1: Four-box conveyor belt model of the ocean. See the text for details.

*Professor, Department of Oceanography University of Hawaii at Manoa Honolulu, HI 96822, USA

第23回海洋化学学術賞受賞（平成20年 4 月28日）

relationships $I_b = I_s$ and $I_b^* = I_s^*$ are implied in a steady state ocean and their residence times in the ocean are relatively long. For the nutrient type elements ($C_0 < C$, $C_0^* < C^*$, and $C < C^*$), $I_b > I_s$ and $I_b^* > I_s^*$. For the scavenged type elements ($C_0 > C$, $C_0^* > C^*$, and $C > C^*$), $I_b < I_s$ and $I_b^* < I_s^*$ and their residence time are short (Li, 2000). For the mixed type elements ($C_0 < C$, $C_0^* < C^*$, and $C > C^*$), the relationships among I_b, I_s, I_b^* and I_s^* are not clear-cut but all have short residence times. The increase of concentration with depth down to the bottom for these mixed type elements may suggest additional inputs of colloidal and dissolved fractions through re-suspension of bottom sediments (Firdaus *et al.,* 2008).

In the following sections, the surface complexation model of ions on hydrated metal oxides and organic matter is presented first. The concept of mean residence time of elements in the ocean and its relationship to the surface complexation model is introduced next. The partition of elements between seawater and algae (representative of all living marine organisms), and between seawater and deep sea manganese nodules are discussed further. Finally, the importance of the elemental fluxes from the mid-ocean ridge hydrothermal vents relative to that from rivers is discussed. The major sinks for dissolved elements in the ocean are mainly marine sediments (pelagic clay, black shale, carbonates, silica, barite, phosphorites, evaporites and mid-ocean ridge metalliferous sediments, etc.), and some escape into the atmosphere as seasalts and methylated gaseous species.

2. The surface complexation model

According to the surface complexation model (Stumm *et al.,* 1970, Schindler 1975), the adsorption of cation M^{z+} on a hydrated metal oxide surface (≡MeOH) can be represented by

$$M^{z+} + \equiv MeOH \leftrightarrow \equiv MeO\text{-}M^{z-1} + H^+ \qquad (1)$$

$$K_1^s = [\equiv MeO\text{-}M^{z-1}]\,[H^+]/[\equiv MeOH]\,[M^{z+}]$$
$$= \{\equiv MeO\text{-}M^{z-1}\}\,[H^+]/\{\equiv MeOH\}\,[M^{z+}]$$
$$= Kd\,[H^+]/\{\equiv MeOH\} = \exp(-\Delta G_{ads}/RT)$$

Here, Me = metal of hydrated metal oxide (e.g. Al, Fe, Mn, Si, Ti).

K_1^s = the first stability constant of cation on hydrated metal oxide surface

$K_d = \{\equiv MeO\text{-}M^{z-1}\}/[M^{z+}]$ = the distribution coefficient of element M

ΔG_{ads} = Gibbs free energy change of the adsorption reaction (1).

[ ] = concentration in mole/l, and { } = concentration in mole/g of suspended solid. [ ] = { } × C_p, where C_p = concentration of suspended solid in g/l.

Log K_1^s or $-\Delta G_{ads}$ is directly proportional to the O-M bond strength between the adsorbed cation and the oxygen of the hydrated oxide surface.

An analogy to reaction (1) is the hydrolysis of cation in water:

$$M^{z+} + H_2O \leftrightarrow M(OH)^{z-1} + H^+ \qquad (2)$$

$$^*k_1 = [M(OH)^{z-1}]\,[H^+]/[M^{z+}] = \exp(-\Delta G_{hyd}/RT)$$

Here, $^*k_1$ = the first hydrolysis constant of cation M^{z+} in water, and ΔG_{hyd} = the Gibbs free energy change of the hydrolysis reaction (2). Log $^*k_1$ or $-\Delta G_{hyd}$ is again proportional to the O-M bond strength between the cation and the oxygen of hydroxyl ligand. Therefore, log $^*k_1$ and log K_1^s for various cations are expected to be linearly related. Similarly for the second cumulative formation constants log $^*\beta_2$ and log β_2^s, where

$$\beta_2^s = \{(\equiv MeO)_2M^{z-2}\}\,[H^+]^2/\{\equiv MeOH\}^2\,[M^{z+}]$$

$$*\beta_2 = [M(OH)_2^{z-2}]\,[H^+]^2/[M^{z+}]$$

Figure 2a shows such a linear relationship (Schindler and Stumm, 1987), based on the log K_1^s and log β_2^s of various cations for amorphous SiO_2 (Schindler, 1975), and log $*k_1$ and log $*\beta_2$ values from Baes and Mesmer (1976). Excluding one data point for Mg, one obtains the following relationship:

$$pK_1^s \text{ (or } p\beta_2^s) = (0.66\pm0.49) + (0.59\pm0.03)\ p*k_1 \text{ (or } p*\beta_2) \qquad (3)$$

Here "p" represents "$-\log$ ", and r^2 is about 0.97.

The extensive data on logarithmic $*k_1$, $*\beta_2$, $*\beta_3$, $*\beta_4$ for various cations as summarized by Baes and Mesmer (1976) are most useful to predict the relative magnitude of logarithmic K_1^s, β_2^s, β_3^s, β_4^s for any hydrated metal oxides. The dotted line in Figure 2b represents the linear relationship:

$$p*\beta_2 = (1.21\pm0.29) + (1.91\pm0.05)\ p*k_1 \qquad (4a)$$

Additional relationships are:

$$p*\beta_3 = (2.27\pm0.33) + (1.42\pm0.03)\ p*\beta_2 \qquad (4b)$$

$$p*\beta_4 = (4.74\pm0.29) + (0.96\pm0.04)\ p*\beta_3 \qquad (4c)$$

According to equations 4a and 4b, the following relationship holds for cations with high log $*k_1$, namely, log $*k_1 \approx (\log *\beta_2)/2 \approx (\log *\beta_3)/3$, or log $K_1^s \approx (\log \beta_2^s)/2 \approx (\log \beta_3^s)/3$. Therefore, the averaged single M-O bond strength obtained from bi-dentate and tri-dentate is similar to that from unidentate. However, this does not hold for tetra-dentate.

Another useful geochemical parameter is the electron binding energy (I_z) to cations. The I_z is defined as the energy released during the spontaneous uptake of electron by gaseous cation $M^{z+}(g)$, namely:

$$M^{z+}(g) + e^- \leftrightarrow M^{z-1}(g) + I_z \qquad (5)$$

The I_z is also called the ionization energy for the reverse reaction. The values of I_1 (the first ionization energy) to I_8 (8^{th} ionization energy) for various gaseous elements and cations can be found in Lide

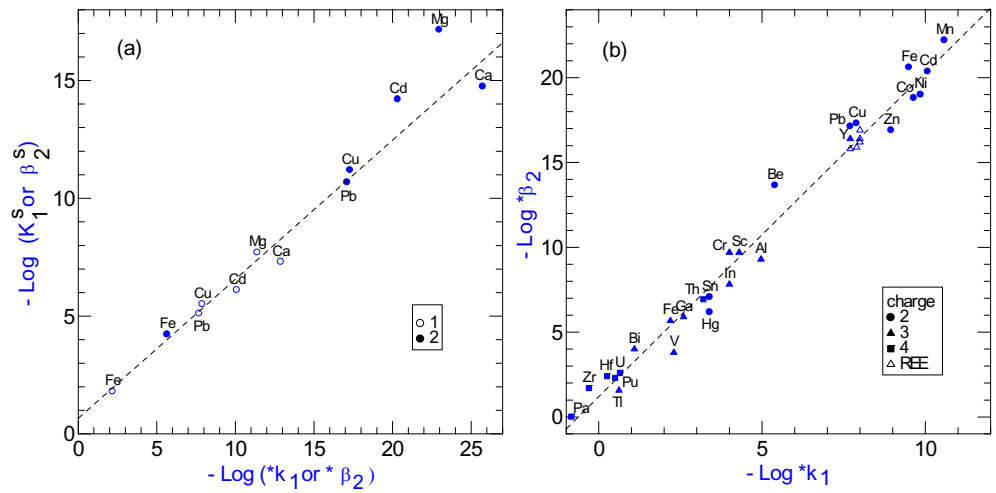

Figure 2: (a) The hydrolysis constants (log $*k_1$ or $*\beta_2$) versus the surface complexation constants on amorphous SiO_2 (log K_1^s or β_2^s) for Mg^{2+}, Ca^{2+}, Cd^{2+}, Cu^{2+}, Pb^{2+}, and Fe^{2+}, (b) The first hydrolysis constants (log $*k_1$) versus the second cumulative hydrolysis constants for various cations with charges 2 to 4.

(2008), Li (2000) and Cotton (1991, for lanthanides and actinides). The I_z are shown to be proportional to the bond strength between cations and an electron-providing ligand (Li, 1981), thus are also proportional to log $*k_1$ (or O-M bond strength), as proven in Figure 3a. A few obvious exceptions are Tl^+, Ag^+, Pb^{2+}, Hg^{2+}, Bi^{3+} (all have the outer-shell electron configuration of d^{10}), and Li^+ and Be^{2+} (each has the smallest ionic radius among alkali and alkaline-earth elements). Apparently, those cations are too low in I_z at a given log $*k_1$. In other words, I_z for those cations underestimates the O-M bond strength. As cautioned by Baes and Mesmer (1976), log $*k_1$ for Na^+ and K^+ also have large uncertainty. Excluding all those exceptions, the relationship between log $*k_1$ and I_z for other cations can be represented by

$$I_z = (33.5 \pm 0.5) + (1.70 \pm 0.07) \log *k_1, \text{ with } r^2 = 0.91 \qquad (6)$$

and is shown as a dotted line in Figure 3a.

Inserting log $*k_1$ values for outlying cations into equation 6 or reading visually from Figure 3a, one obtains the "effective" electron binding energy $*I_z$ for $Li^+ = 10$, $Tl^+ = 11$, $Ag^+ = 13$, $Pb^{2+} = 20$, $Be^{2+} = 24$, $Hg^{2+} = 26$, $Bi^{3+} = 32$ eV, with an uncertainty of ~10 %. Since log $*k_1$ values for oxy-cations and ions $B(OH)_3^0$, NpO_2^+, PuO_2^{2+}, RuO_4^0, $Ti(OH)_2^{2+}$ and UO_2^{2+} are also known (Baes and Mesmer, 1976), their $*I_z$ values are again roughly estimated to be 17, 18, 24, 14, 30 and 20 eV respectively (again with uncertainty of ~10 %). As examples, the hydrolysis reactions of $B(OH)_3^0$ and $Ti(OH)_2^{2+}$ are:

$$B(OH)_3^0 + H_2O \leftrightarrow B(OH)_4^- + H^+; \quad Ti(OH)_2^{2+} + H_2O \leftrightarrow Ti(OH)_3^+ + H^+.$$

Figure 3b provides additional proof that I_z and log β_1 for organic ligand EDTA (ethylenediaminetetraacetic acid, which contains functional groups −OH and =NH) or the bond strength between cations and EDTA (L^{4-}) are positively related. Here β_1(EDTA) is defined as

$\beta_1(\text{EDTA}) = [ML^{z-4}]/([M^{z+}][L^{4-}])$ for a complex forming reaction of

$$M^{z+} + L^{4-} \leftrightarrow ML^{z-4}$$

The I_z values for d^{10} cations Pb^{2+}, Sn^{2+}, Hg^{2+}, and Bi^{3+} are again too low at given log β_1(EDTA) values.

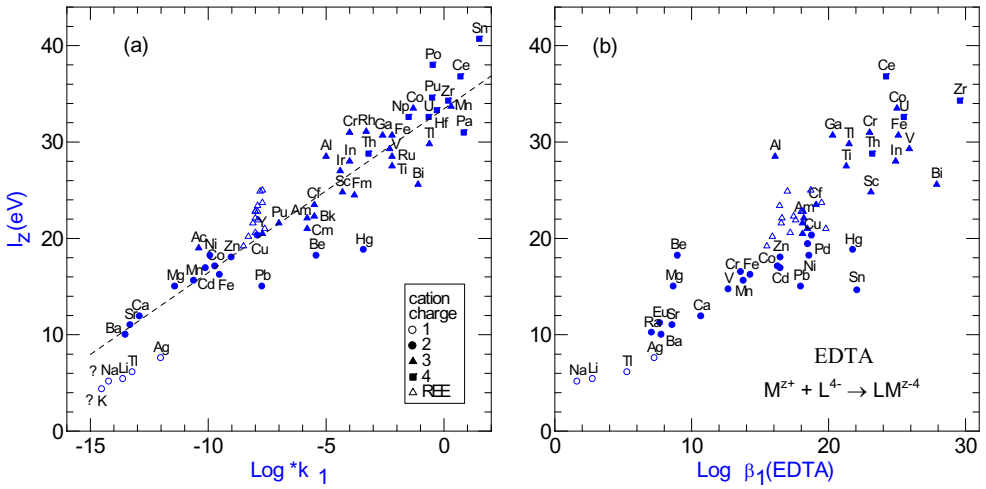

Figure 3: (a) The first hydrolysis constants (log $*k_1$) of cations, and (b) the first complexation constants of cations to organic ligand EDTA against the electron binding energy (I_z) to various cations M^{z+} with charges 1 to 4.

From Figures 3a and 3b, one also can easily see the linear relationship between log $*k_1$ and log β_1 (EDTA) or any other organic ligands (Balistrieri *et al.,* 1981). The advantage of using I_z over log $*k_1$ is that there are more data on I_z than on log $*k_1$ for various cations. In short, I_z of cations are positively correlated with log $*k_1$, log K_i^s, and log K_d of cations at given pH and {≡MeOH}.

Historically, the concept of ionic potential (= z/r; where z = charge of ion, and r = crystal ionic radius; see Li, 2000 and references therein) was widely utilized to explain geochemical behaviors of elements (e.g. Ishibashi and Shigematsu, 1951; Andrews *et al.,* 1981). However, as shown in Figure 4, the correlation of log $*k_1$ or log β_1(EDTA) with z/r is not as tight as with I_z (Figure 3).

According to the surface complexation model, the adsorption of phosphate (as an example of oxyanions) on hydrated metal oxides can be represented by:

$$H_2PO_4^- + \equiv MeOH \leftrightarrow \equiv Me\text{-}O\text{-}PO_3H_2 + OH^- \quad (7)$$

$$K_{a1}^s = \{\equiv Me\text{-}O\text{-}PO_3H_2\}\,[OH^-]/([H_2PO_4^-]\,\{\equiv MeOH\})$$

$$= K_d\,[OH^-]/\{\equiv MeOH\} = \exp(-\Delta G_{ads}/RT).$$

Here K_{a1}^s = the complexation constant of $H_2PO_4^-$ on hydrated metal oxide,

$K_d = \{\equiv Me\text{-}O\text{-}PO_3H_2\}/[H_2PO_4^-]$ = the distribution coefficient of $H_2PO_4^-$,

ΔG_{ads} = Gibbs free energy change for the adsorption reaction (7).

Log K_{a1}^s or $-\Delta G_{ads}$ is proportional to the bond strength between the surface metal of solid oxide and oxygen of oxyanion (Me-O).

The analogy to the reaction (7) is

$$H_2PO_4^- + H_2O \leftrightarrow H\text{-}O\text{-}PO_3H_2 + OH^- \quad (8)$$

$$K_1' = [H_3PO_4]\,[OH^-]/[H_2PO_4^-] = K_w / K_1.$$

Here K_1' = hydrolysis constant of oxyanion.

K_w = water dissociation constant = $[H^+][OH^-]$, and

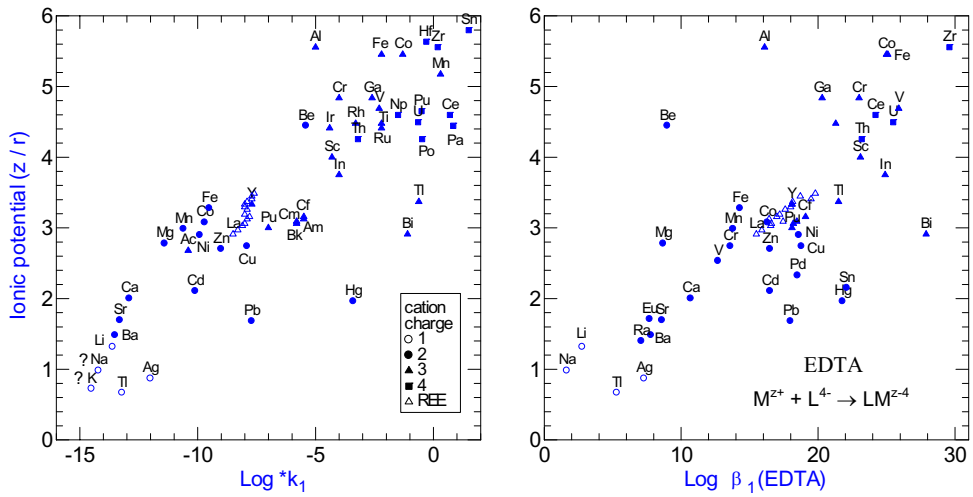

Figure 4: (a) The first hydrolysis constants (log $*k_1$) of cations, and (b) the first complexation constants of cations to organic ligand EDTA against the ionic potential (z/r) of various cations.

K_1 = the first dissociation constant of phosphoric acid = $[H_2PO_4^-][H^+]/[H_3PO_4]$.

Therefore, log K^s_{a1} should be proportional to log K_1' and inversely proportional to log K_1. Similarly, one may predict the inverse relationship between log K^s_{a2} (complexation constant of HPO_4^{2-}) and log K_2 (second dissociation constant of phosphoric acid), and between log K^s_{a3} (complexation constant of PO_4^{3-}) and log K_3 (third dissociation constant of phosphoric acid). Figure 5a confirms these inverse relationships for oxyanions of As(V), P(V), and Se(IV). Log K^s_{ai} for those oxyanions on goethite (sample C) are obtained from Goldberg (1985, 1986). Figure 5b demonstrates again the linear relation between log K_1 and log K_2 for various oxy-acids with this relationship:

$$\text{Log } K_2 = (-5.27 \pm 0.23) + (0.78 \pm 0.04) \log K_1, \qquad (10)$$

and $r^2 = 0.96$

There are only a few data on log K_3 to make any meaningful correlation with log K_2. Adsorption of the simple anion Br^- (as well as F^- and Cl^-) can be represented by:

$$Br^- + \equiv MeOH \leftrightarrow \equiv Me\text{-}Br + OH^- \qquad (11)$$

$$K^s_{a1} = \{\equiv Me\text{-}Br\}[OH^-]/([Br^-]\{\equiv MeOH\})$$

One can easily demonstrate that log K^s_{a1} for F^-, Cl^-, and Br^- are again inversely related to log K_1 for HF, HCl and HBr acids. The I^- ion is excluded here, since the major species of iodine is IO_3^- in seawater.

Finally, Figure 6 shows the general positive correlation between log K_1 of various oxy-acids and I_z values of the central metals in oxyanions. For example, the central metal of PO_4^{3-} is P(V). Apparently, the higher is the I_z of the central metal of oxyanion, the stronger is the bond strength between the central metal and the oxygen of oxyanion (M-O), and the weaker is the bond strength between the oxygen of oxyanion and hydrogen ion (M-O-H; thus strong acid) or the surface metal of hydrated oxides (M-O-Me). From the log K_1 values for HCl, HBr, and HF, one can also roughly

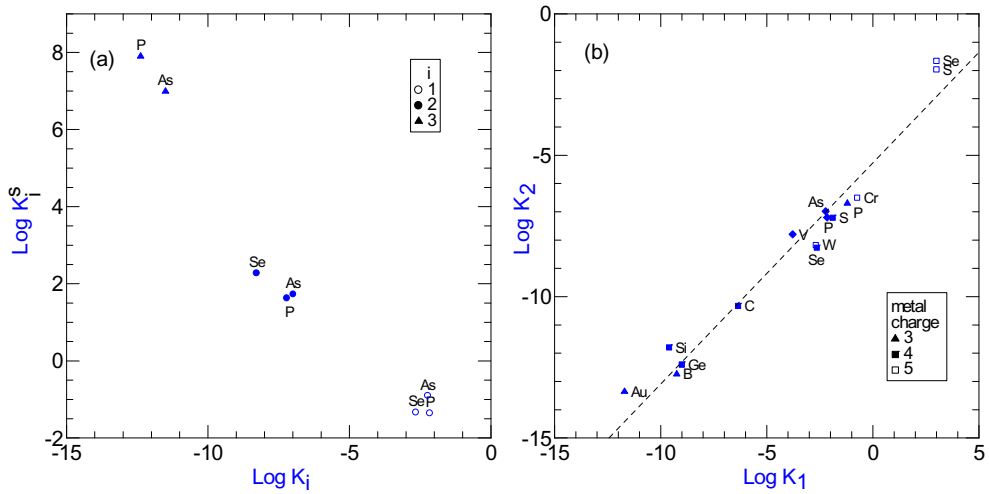

Figure 5: (a) Log K_i (step-wise dissociation constants of oxyacids H_3AsO_4, H_3PO_4, H_2SeO_3; i = 1, 2, and 3) versus log K^s_i (step-wise complexation constants of oxyanions on goethite), and (b) log K_1 (the first dissociation constants) versus log K_2 (the second dissociation constants) of oxyacids of various metals.

estimate from Figure 6 the effective electron binding energy $^*I_z$, which are about 100 eV for Cl^- and Br^-, and 70 eV for F^-. In short, I_z of the central metals in oxyanions and $^*I_z$ of simple anions are positively correlated to their log K_1 and inversely correlated with log K^s_{a1} or log K_d at given pH and {≡MeOH}. Therefore I_z and $^*I_z$ are useful parameters to relate the extent of adsorption of both cations and anions on the surface of natural particles in any aquatic system.

3. Partition of elements between water and suspended particles in rivers.

The average concentrations of elements in the world's average river water (C_R, in units of μg/l) and river suspended particles (X_R, in units of μg/g) are summarized by Martin and Whitfield (1981) and up-dated by Li (2000). However, the rare earth elements (REE), Y, and Re data are adopted from the recent estimates by Gaillardet *et al.* (2003). The Hg is from Tseng *et al.* (2004). The C_R data for Ag and Au are not reliable as noted by Li (2000), therefore they are excluded from the following discussion. Since the average composition of the river-suspended particles is essentially the same as that of the world's average shale (X_{sh};

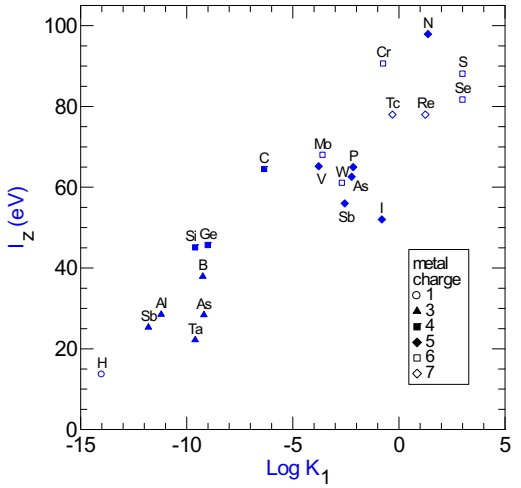

Figure 6: The correlation between log K_1 (the first dissociation constants of oxyacids) and the electron binding energy of the central metal of oxyanions.

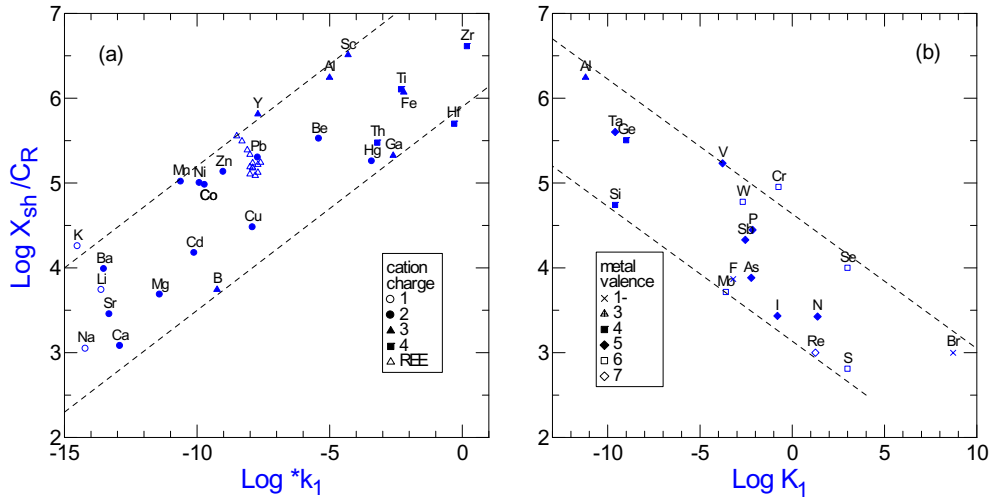

Figure 7: (a) The positive correlation between log $^*k_1$ (the first hydrolysis constants of various cations) and log X_{sh}/C_R (where X_{sh} = concentrations of elements in the world's average shale, and C_R = concentrations of elements in the world's average river water), and (b) the negative correlation between log K_1 (the first dissociation constants of various oxyacids) and log X_{sh}/C_R. Tow parallel dotted lines show general correlation trends.

Li, 2000), the average shale is adopted here to represent the unpolluted river suspended particles, and to include more elements.

As shown in Figure 7, log X_{sh}/C_R ratios (bulk distribution coefficients) of mono- to tetra-valent cations are, in general, positively correlated with their log $^*k_1$ (the first hydrolysis constants), and the log X_{sh}/C_R of oxyanions, F^-, and Br^- are inversely correlated with their log K_1 (the first dissociation constants of oxyacids and acids) values. The double dotted lines in Figure 7 (about one to two orders of magnitude apart) show the general positive and negative correlation trends. The log X_{sh}/C_R for Cr is high at the given log K_1 value for H_2CrO_4 (Figure 7b), probably caused by the existence of Cr (III) species as well. For example in seawater, the concentration ratio of Cr(VI)/Cr(III) is about 100 (Li, 2000), but the ratio of the distribution coefficients between Cr(VI)/Cr(III) is about 1/100 (Santschi *et al.,* 1987). Therefore, the adsorption of both Cr(VI) and Cr(III) are important in sediments. In order to include the effect of both Cr(VI) and Cr(III), the "apparent effective charge" of Cr is assigned to be (IV). The concentration ratio of Se(VI)/Se(IV) is about 1.6 in seawater, and their distribution coefficients should not differ as much as two orders of magnitude. Therefore, both Se(VI) and Se(IV) are also important species in water and sediments, and the apparent effective charge for Se is assigned to be (V) hereafter. The concentration ratio of As(V)/As(III) in seawater is about 330 (Li, 2000), thus any effect by As(III) can be ignored.

In the plot of log X_{sh}/C_R versus I_z (Figure 8), the $^*I_z$ values are adopted for the elements with asterisk (as well as in many following figures), and I_z values for Cr and Se are based on their apparent effective charges. The double dotted lines in Figure 8 (about one to two orders of magnitude apart) also show the general positive and negative correlation trends. The obvious exceptions to the trends

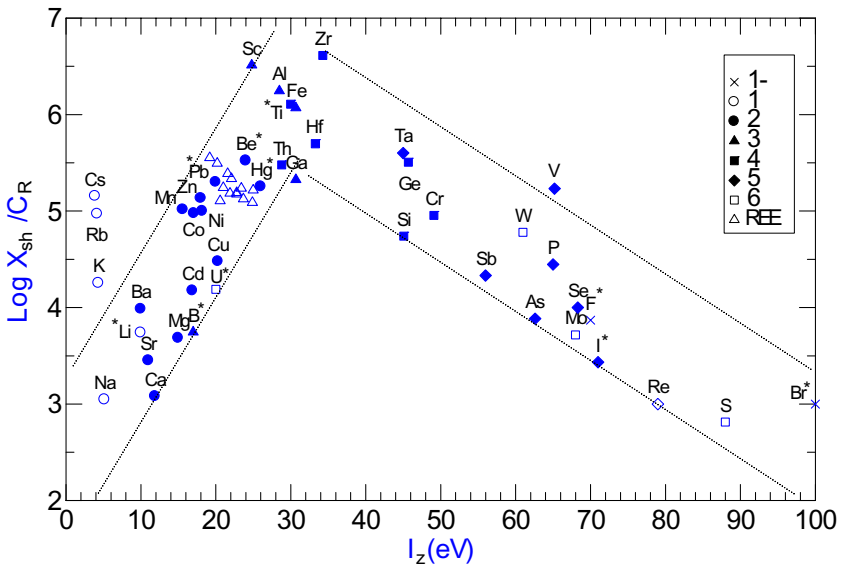

Figure 8: The up-and-down "Λ" relationship between I_z and log X_{sh}/C_R for cations and anions. $^*I_z$ values are adopted for the elements with asterisk (such as Li, Be, B, Pb, Ti, F, Br, and I) for this and all following figures. The outlying Cs, Rb and K (outside of two parallel dotted lines) are due to the secondary solvation energy effect (see the text for detail).

are alkali and alkaline earth elements. Especially, the log X_{sh}/C_R values decrease drastically from Cs to Na, when I_z increases only slightly (Figure 8). A possible explanation follows: The ionic potential (z/r) of Cs is much smaller than that of Na (due to the increasing order of ionic radius from Na to Cs), thus its hydration waters are less tightly held. Therefore, during the adsorption process, the hydration waters of Cs can be easily removed, enhancing the adsorption, and results in the log X_{sh}/C_R values in the observed order of Cs > Rb > K > Na. The energy spent in removing hydration water during the adsorption process is called the secondary solvation energy (James and Healy, 1972). Similar explanation may also apply to alkaline earth elements. For Li^+ and Be^{2+} (each has the smallest ionic radius among alkali and alkaline earth elements), their $^*I_z$ values are large enough to overshadow the secondary solvation energy effect. The up-and-down relationship between log X_{sh}/C_R and I_z in Figure 8 is called the "Λ" (Greek capital letter lambda) relationship throughout this paper.

4. Mean residence times of elements in the ocean.

The mean residence time τ_i (or mean replacement time) of a given element *i* in the ocean from river input is defined (Barth, 1952):

$$\tau_i \text{ (years)} = V_O \cdot C^i_{SW}/F_R \cdot C^i_R = 38000\ C^i_{SW}/C^i_R, \text{ or} \qquad (11a)$$

$$\kappa_i = 1/\tau_i \propto C^i_R/C^i_{SW} \qquad (11b)$$

Here, C^i_R and C^i_{SW} = average concentrations of dissolved element *i* in rivers and seawater.

V_O = volume of ocean = $1.4 \cdot 10^{21}$ liters

F_R = river runoff = $37 \cdot 10^{15}$ liters / year

κ_i = the first order removal rate constant of element *i* from the ocean to sediment sinks or the reactivity of element *i* to sediments.

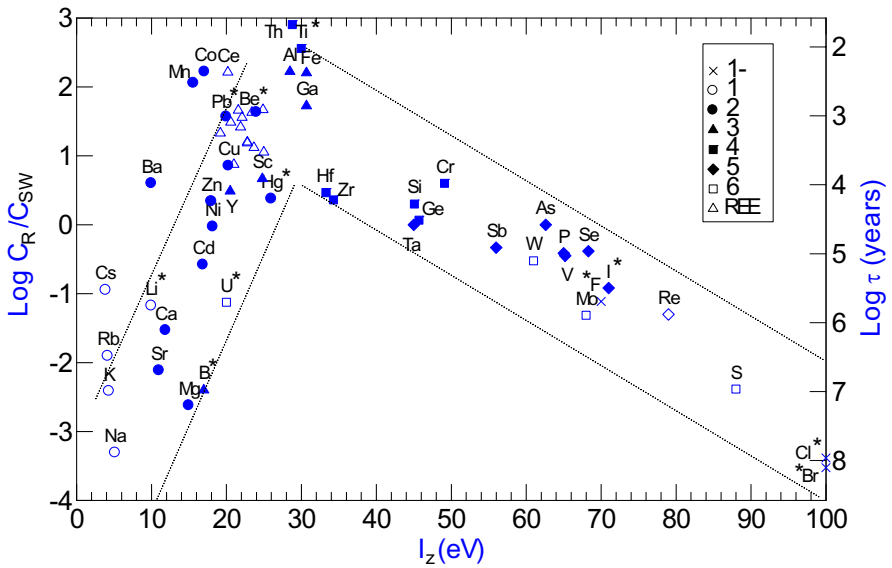

Figure 9: The "Λ" relationship between I_z and log C_R/C_{SW} (C_{SW} = concentrations of elements in seawater) for cations and anions. The outlying values of Mn, Co, and Ce are due to the additional oxidative removal in the ocean, and the Ba, Cs, and Rb are due to the secondary solvation energy effect (see the text for detail).

The C^i_{SW} data are from Li (2000). One should keep in mind that the recent estimates on the concentrations of Hf, Nb, Ta, and W in the North Pacific Ocean are about one order of magnitude lower (Sohrin *et al.,* 1998; Firdaus *et al.,* 2008). Before adopting these new values, one needs also to measure those elements in the Atlantic Ocean and to improve corresponding values for river waters. The higher is the log C^i_R/C^i_{SW} ratio, the more reactive is the element, and the shorter is its mean residence time in the ocean, and vice versa.

The plot of log C^i_R/C^i_{SW} (or $-\log \tau_i$) versus I_z (and $*I_z$ for some elements with asterisk) in Figure 9 again clearly shows the up and down "Λ" relationship. The implication is that the relative reactivity of elements in the ocean is, for the first approximation, controlled by the bond strengths between the adsorbing cations and the oxygen of the hydrated metal oxides, and between the adsorbing oxyanions and the metal of the hydrated metal oxides in the ocean. The relatively high log C^i_R/C^i_{SW} values for Mn, Co and Ce at given I_z may indicate additional oxidative removal ($Mn^{2+} \rightarrow Mn^{4+}$; $Co^{2+} \rightarrow Co^{3+}$; and $Ce^{3+} \rightarrow Ce^{4+}$) at the sediment-water interface in the deep ocean to reduce C^i_{SW} values. The high log C^i_R/C^i_{SW} values for Ba and Cs may also indicate effective removal of Ba and Cs in the ocean, which will be discussed later.

Goldberg and Arrhenius (1958) introduced another way to define the mean residence time of elements in the ocean, using output rates of elements to the ocean pelagic clay, namely:

$$\tau^*_i \text{ (years)} = V_O \cdot C^i_{SW}/(F_{op} \cdot X^i_{op}) \propto C^i_{SW}/X^i_{op} \qquad (12a)$$

or $$1/\tau^*_i \propto X^i_{op}/C^i_{SW} \qquad (12b)$$

where F_{op} = sedimentation rate of the ocean pelagic clay = $1.1 \cdot 10^{15}$ g/y, and X^i_{op} = the average con-

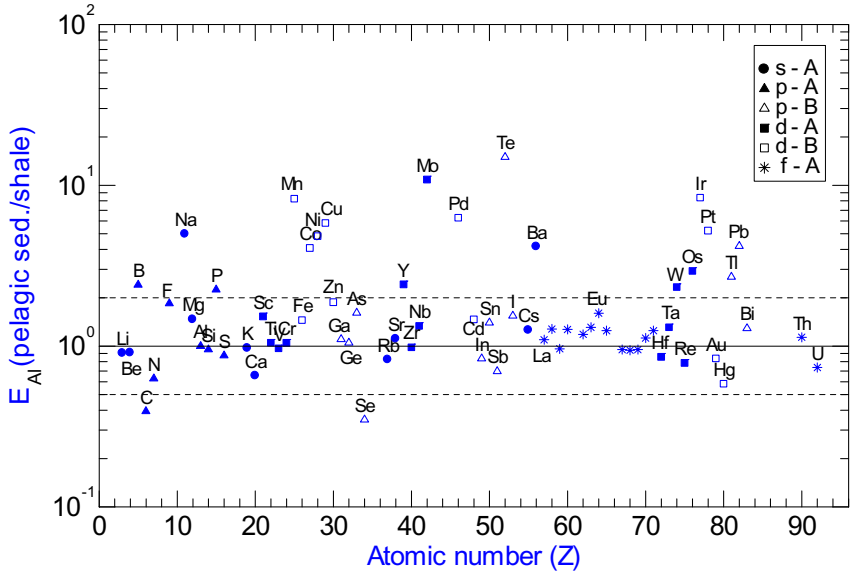

Figure 10: The enrichment factors of elements in the average ocean pelagic sediments (as compared with the world's average shale and normalized to Al) as a function of their atomic number (Z). The elements are classified according to their outermost electron subshells (s, p, d, and f) and their cationic electron configurations (A type = electron configuration of noble gases and f^{1-14}, and B type = d^{1-10}). The elements within the two dotted horizontal lines have E_{Al} values between 1/2 to 2.

centration of element i in the ocean pelagic clay (10^{-6} g/g).

The average composition of ocean pelagic clay is given by Li (2000), and is similar to that of the shale, mostly within a factor of 2 as shown by the enrichment factor calculation (Figure 10). The enrichment factor is defined as the concentration ratio of element i and the normalizing element j (X_i/X_j) in a given sample divided by the same ratio in a chosen reference material, i.e.

$$E_j^i(\text{sample/reference}) = \frac{(X_i/X_j)_{\text{sample}}}{(X_i/X_j)_{\text{reference}}} \qquad (13)$$

In the present case, Al is taken as the normalizing element, and the shale as the reference material. However, the elements Na, Mn, Co, Ni, Cu, Mo, Pd, Te, Ba, Os, Ir, Pt, Tl, and Pb are very much enriched in ocean pelagic clay as compared with shale (Figure 10). As shown by Li and Schoonmaker (2003), those enriched elements are mainly associated with the manganese oxide coating on the pelagic clay particles according to the factor analysis.

The plot of log X_{op}^i/C_{SW}^i versus I_z (Figure 11) again exhibits the "Λ" relationship. The relatively high log X_{op}^i/C_{SW}^i values for Mn, Co, Ce, Pb, and Tl again indicate additional oxidative uptake of those elements on the particle surface (Li, 1991, 2000; $Mn^{2+} \rightarrow Mn^{4+}$, $Co^{2+} \rightarrow Co^{3+}$, $Pb^{2+} \rightarrow Pb^{4+}$, $Ce^{3+} \rightarrow Ce^{4+}$, $Tl^{+} \rightarrow Tl^{3+}$). The high log X_{op}^i/C_{SW}^i values for Cs, Rb, and Ba reflect the secondary salvation energy effect as discussed earlier (James and Healy, 1972). Barium also can be removed effectively in the ocean as barite ($BaSO_4$).

The close relationship between log X_{op}^i/C_{SW}^i (or $-\log \tau^*$) and log C_R^i/C_{SW}^i (or $-\log \tau$) is evident in Figure 12. The rankings of relative reactivity of elements obtained by river inputs and sediment outputs are similar, even though for most of the elements τ is not equal to τ^* (the dotted line in Figure

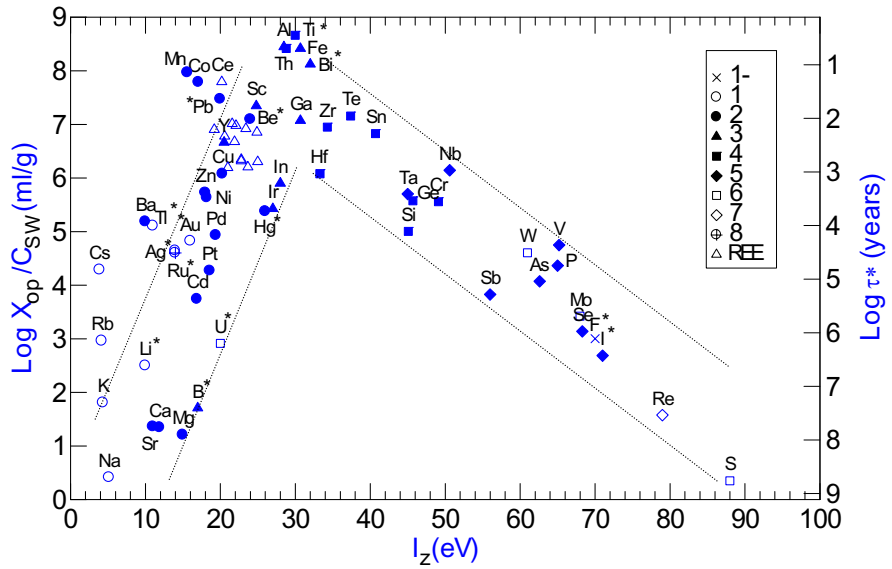

Figure 11: The "Λ" relationship between I_z and log X_{op}/C_{SW} (X_{op} = concentrations of elements in ocean pelagic sediments) for cations and anions. The additional oxidative uptakes for Mn, Co, Ce, Pb, and Tl, and the secondary solvation energy effect for Cs, Rb, and Ba are present.

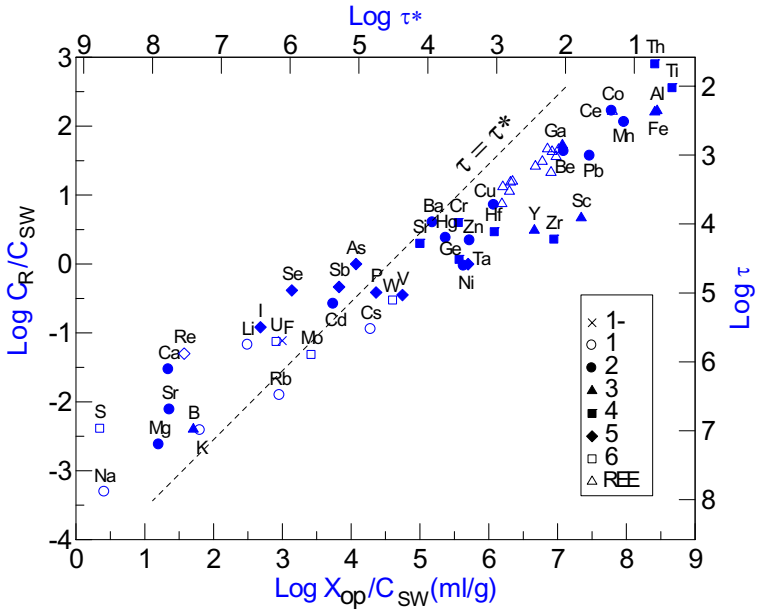

Figure 12: The correlation between log X_{op}/C_{SW} and log C_R/C_{SW} for various elements. The dotted line represents $\tau = \tau^*$ (τ are the mean residence times of elements based on river inputs, and τ^* based on the sediment outputs).

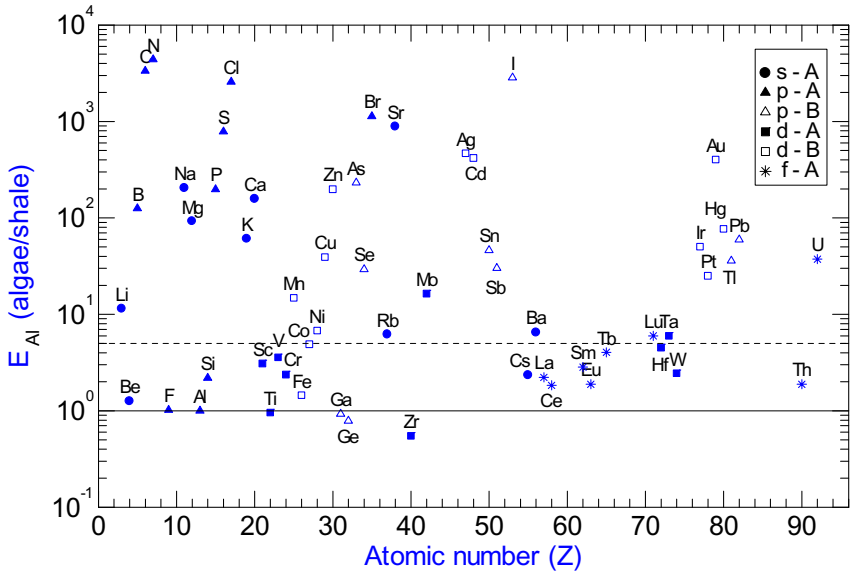

Figure 13: The enrichment factors of elements in the average marine algae (as compared with the world's average shale and normalized to Al) as a function of their atomic number (Z). The elements with $E_{Al} \sim 1$ to 5 (below the dotted line) are called the biophobic, and $E_{Al} > 5$ the biophilic elements.

12 represents $\tau = \tau^*$). For elements Na, S, Se, Ca, Sr, Mg, I and U, τ^* are greater than τ, indicating the ineffectiveness of ocean pelagic clay in removing those elements in the ocean. It is well known that Na and some S and Ca are removed as evaporates in lagoon environments; S, Se, and U are mainly removed in reducing environments; Ca, Sr, and some Mg are removed as carbonates; Mg is also effectively removed in the hydrothermal systems of the mid-oceanic ridges; and I is recycled through the atmosphere (Li, 2000). For elements with $\tau^* < 10^4$ years, τ^* are always less than τ. The reason is that X_{op} not only include the surface adsorbed component but also detritus components, which are not actively involved in the adsorption/desorption cycles.

5. Affinity of ions to organisms.

As shown by Li (1984, 1991), the chemical compositions of marine and terrestrial organisms are all similar, thus marine algae is selected here to represent all organisms (X_{org}). The average composition of marine algae is mainly from Yamamoto (1983) and is summarized by Li (2000) along with data for other organisms. In Figure 13 (E^i_{A1} (algae/shale) versus atomic number Z), the elements with E^i_{A1} about 1～5 are called the biophobic, and those with $E^i_{A1} > 5$ the biophilic elements (Li, 1984). The biophobic elements may include Be, F, Al, Si, Sc, Ti, Cr, Fe, Ga, Ge, Zr, Cs, REE, and Th. Their relative abundances in algae are similar to those in the shale. In addition, the factor analysis of algae data shows that those biophobic elements co-vary together (Li, 2000, 2006). The implication is that those biophobic elements are mostly incorporated into algae together as inorganic colloidal particles. The biophilic elements are mainly the A-type ions (electron configuration of noble gases or outermost sub-shell of f^{1-14}) that belong to the conservative type with long mean residence time (such as Li, Na, K, Rb, Mg, Ca, Sr, Cl, Br, S, B, Mo, and U), major nutrient type ions (C, N, P), and B-type

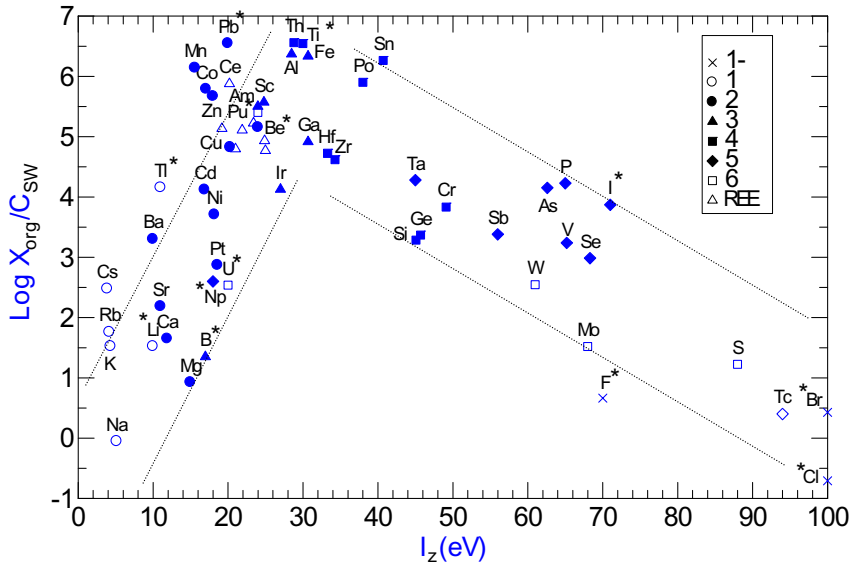

Figure 14: The "Λ" relationship between I_z and log X_{org}/C_{SW} (X_{org} = concentrations of elements in marine algae) for cations and anions. The outlying Mn, Co, Ce, Pb and Tl are due to the additional oxidative removal on the cell surface, and Ba, Cs, Rb are due to the secondary solvation energy effect (see the text for detail).

cations (outermost sub-shell of d^{1-10}, which have high electric polarizability values, especially for d^{10} cations; Li, 2000). The A- and B-type cations here correspond roughly to the "hard" and "soft" cations of Stumm and Morgan (1981). The enrichment of B-type cations in algae as compared with shale particles may reflect the extra strong chemical bonding between B-type cations and hydrophilic functional groups of proteins, such as -SH, $-CH_3$, $-NH_2$, and =PH etc. (in addition to -COOH, -OH) on the cell surface of algae (Li, 1984, 2006; Buffle, 1988). As shown by Li (2000), the electric polarizability values for S^{2-}, C^{4-}, N^{3-}, and P^{3-} (in increasing order) are much higher than that for O^{2-}. Organic ligands containing functional groups -SH, $-CH_3$, $-NH_2$, and =PH correspond to the so-called the "soft", and -COOH and -OH to the "hard" ligands (Buffle, 1988).

The plot of log X_{org}/C_{SW} versus I_z (Figure 14) also shows the "Λ" relationship and indicates the first order thermodynamic control of the partition of elements between algae and seawater. The high log X_{org}/C_{SW} values for Mn, Co, Ce, Pb and Tl again indicate the additional oxidative uptake at the cell surface. The secondary solvation effect is also evident for Cs, Rb and Ba. The log X_{org}/C_{SW} values for radioactive Am, Po, Pu, Np and Tc are summarized by Li (1991, and references therein).

6. Partition of elements between Mn-nodules and seawater

The average composition of deep-sea manganese nodules (X_{mn}) is given by Li (2000, 2003), and the enrichment factor E^i_{Al}(nodule/shale) as a function of atomic number Z is shown in Figure 15. Based on the factor analysis of nodule data, nodules consist of four major components: detritus shale particles, Mn oxides, Fe oxides, and phosphates (Li, 1982, 2003). Association of different elements with different components is also shown in Figure 10. Those assigned associations are based on the factor analysis and/or correlation coefficient calculations. The elements that associate strongly with the iron-oxide phases of nodules exist in normal seawater mainly as hydroxyl and carbonate com-

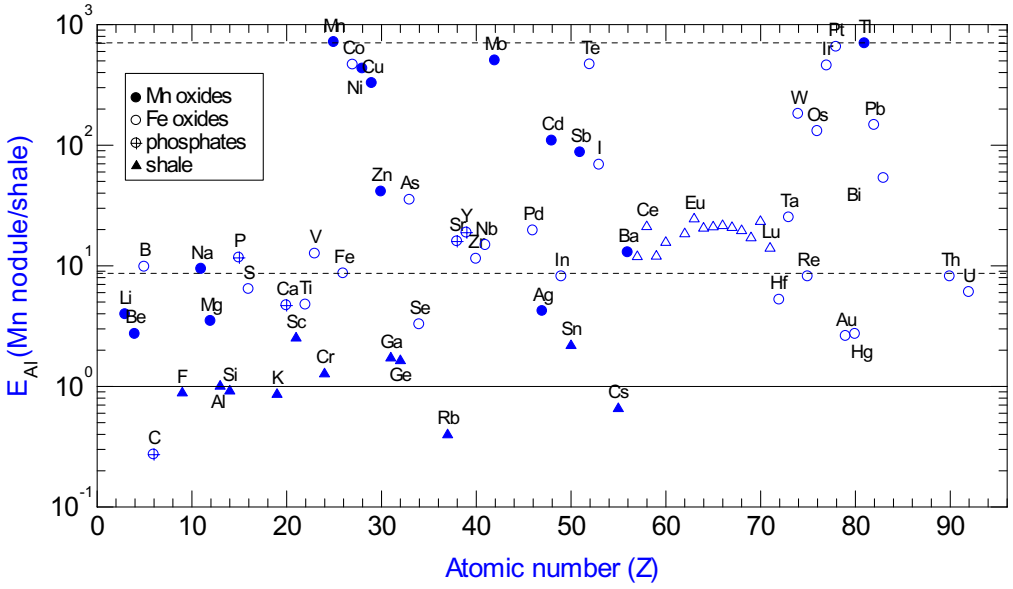

Figure 15: The enrichment factors of elements in the average marine manganese nodules (as compared with the world's average shale and normalized to Al) as a function of their atomic number (Z). The horizontal dotted lines pass through the data points of Fe and Mn.

plexes of tri- to penta-valent cations (e.g., B, Bi, In, Ir, Rh, REE, Y, Ti, Th, U, Zr, Hf, Nb, and Ta), oxyanions (e.g., As, I, P, Re, Ru, Os, S, Se, Te, V, and W), and divalent cations with the high first hydrolysis constants and high tendency to be oxidized to higher valences (Hg, Au, Pd, Pt, Co, and Pb). Carbonate fluorapatite is often closely related to the iron-oxide phases in manganese nodules and contributes significant amounts of Ca, Sr, P, C, REE, and Y in manganese nodules. The E^{i}_{A1} values of near "1" for Si, K, Na, F, Cr, Rb, Cs, Sc, Ga, Sn, and Ge (Figure 10) suggest that those elements are contributed mainly by the detritus shale component in nodules. The Mn-oxide phases concentrate mainly mono- and divalent cations (Li, Na, K, Rb, Cs, Ag, Tl, Be, Mg, Ba, Ni, Cu, and Zn), and oxyanions of Mo and Sb.

Despite of four variable components in Mn-nodules, the plot of log X_{mn}/C_{sw} versus I_z shows the regular "Λ" relationship (Figure 16). The oxidative uptake of Mn, Co, Ce, and Tl; and the secondary solvation effect for Cs, Rb, and Ba are again evident during the growth of manganese nodules.

7. Hydrothermal vent solutions from the mid-ocean ridges

The chemical composition of hydrothermal vent solution (C_{HY}) from a vent called the Hanging Garden on the mid-Pacific Rise at 21° N (Von Damm, 1995) was chosen for the illustration purpose here (Li, 2000). As compared with seawater (Figure 17), the vent solution is extremely depleted in Mg and U, and moderately depleted in F, P, and S. The changes in Na, Cl, Br, Ca, and Sr are minor, and the rest of elements are highly enriched in the vent solution.

The condition for the input of an element from hydrothermal vents to be greater than that from rivers is:

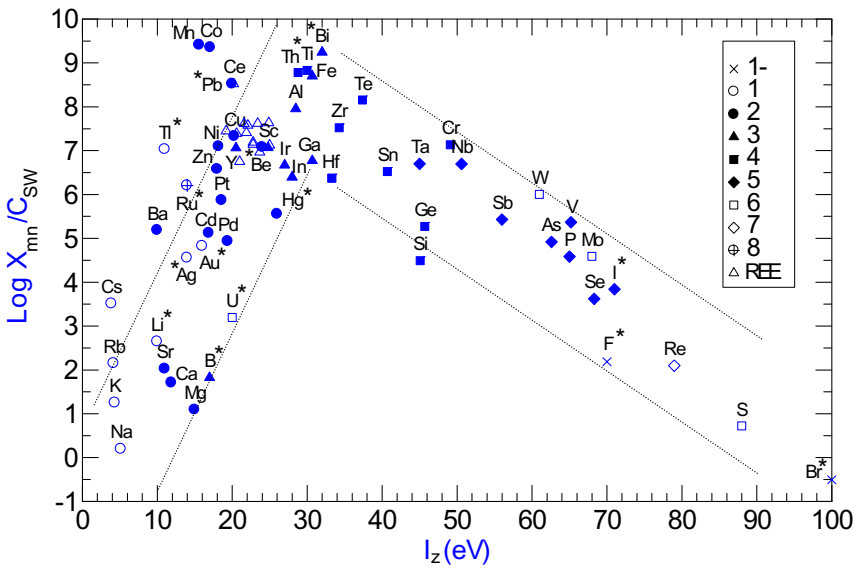

Figure 16: The "Λ" relationship between I_z and log X_{mn}/C_{SW} (X_{mn} = concentrations of elements in manganese nodules) for cations and anions. The outlying Mn, Co, Ce, Pb and Tl are due to the additional oxidative removal at the nodule surface, and Ba and Cs due to the secondary solvation energy effect (see the text for detail).

$$(C_{HY} - C_{SW}) \cdot F_V \geq C_R \cdot F_R \quad (14a)$$

or $$(C_{HY} - C_{SW})/C_R \geq F_R/F_V = 2800, \quad (14b)$$

if the hydrothermal vent flux $F_V = 13 \cdot 10^{15}$ cm^3/yr is adopted (Morton and Sleep, 1985; Chan *et al.*, 1992). If one assumes $C_{SW} \cdot F_V = C_R \cdot F_R$ for Mg (i.e., all Mg input from river to be removed by hydrothermal vent systems), then $F_R/F_V = 420$ (or $F_V = 88 \cdot 10^{15}$ cm^3/yr). As shown in Figure 18, at $F_R/F_V = 2800$, only Zn, Mn, and Fe have higher inputs from vents than from rivers. At $F_R/F_V = 420$, additional vent inputs of Li, Cu, Rb, Cd, Cs, and Pb become more important than river inputs. Certainly one urgently needs to better constrain the F_V estimate.

The extent of leaching of elements from the mid-ocean ridge basalt (MORB) by hydrothermal vent solutions can be represented by the X_{MORB}/C_{HY} ratios (here X_{MORB} = concentrations of elements in the mid-ocean ridge basalt; summarized by Li, 2000). A high ratio indicates low leaching, and vice versa. Interestingly, the plot of log X_{MORB}/C_{HY} versus I_z again shows the "Λ" relationship (Figure 19). Exceptionally low log X_{MORB}/C_{HY} values for Mn, Pb, Cd, Cu and Zn may indicate the formation of stable polysulfide complexes and enhance their solubility in the vent solution. The low X_{MORB}/C_{HY} value for Eu reflects the higher solubility of divalent Eu than of other trivalent REE in the anoxic vent solution. The secondary solvation effect and the oxidative uptake process are apparently not important during the leaching of the MORB by hydrothermal solutions.

When the anoxic vent solution mixes with oxic seawater, dissolved Fe^{2+} and Mn^{2+} are oxidized, and Fe- and Mn- oxide precipitates are accumulated over the mid-oceanic ridge and flank. The enrichment pattern of various metals in the ridge sediments is shown in Figure 20a (as E^i_{A1}(ridge sediments/shale) versus atomic number Z). The question is how much of metals are contributed directly from the hydrothermal vent solutions and how much are scavenged from seawater by Fe- and Mn-

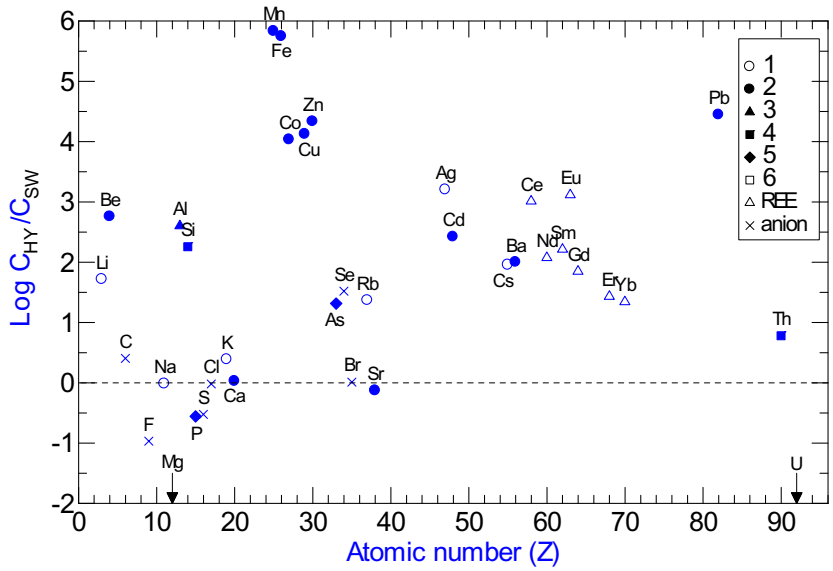

Figure 17: The atomic number (Z) versus log C_{HY}/C_{SW} (C_{HY} = concentrations of elements in hydrothermal vent solution from the Hanging Garden vent, the mid-Pacific ocean ridge, 21° N. The C_{HY} for Mg and U are almost undetectably small.

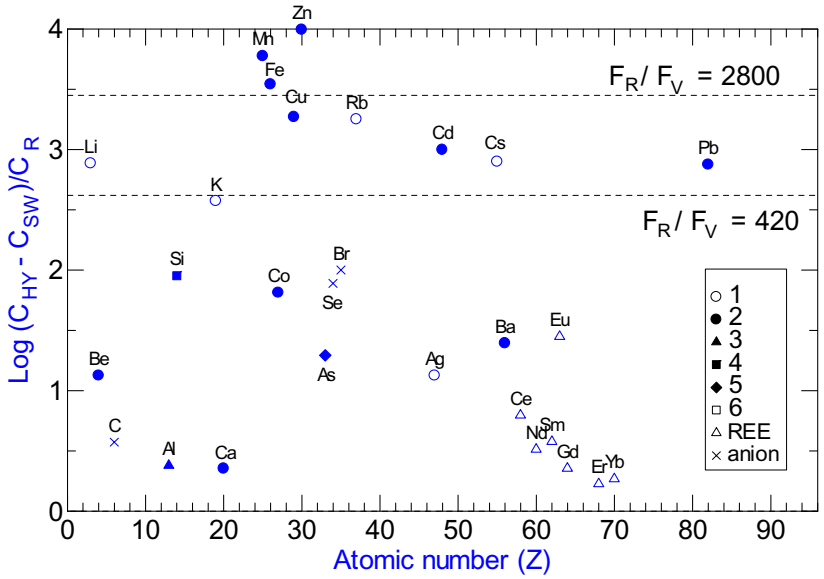

Figure 18: The atomic number (Z) versus log $(C_{HY}-C_{SW})/C_R$. The horizontal dotted lines are log $(C_{HY}-C_{SW})/C_R$ values corresponding to $F_R/F_V = 420$ and 2800 (F_R and F_V are respectively the average river and hydrothermal solution fluxes into the ocean).

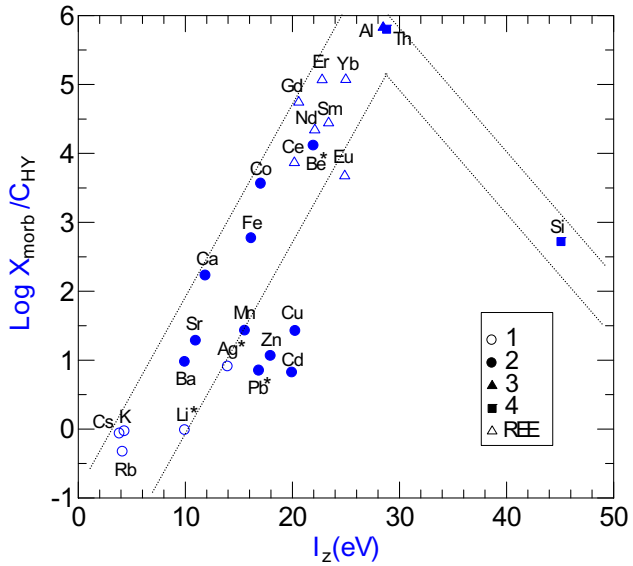

Figure 19: The "Λ" relationship between I_z and log X_{morb}/C_{HY} (X_{morb} = average concentrations of elements in the mid-ocean ridge basalts) for cations and Si. The low log X_{morb}/C_{HY} values for Ag, Cd, Cu, Pb and Zn may indicate the formation of polysulfide complexes to increase their solubility in vent solutions. Part of Eu exists as Eu^{2+} in the anoxic vent solution.

oxide precipitates. Assuming all Mn in the ridge sediment to be of vent input origin and when

$(X_i/X_{Mn})_{sed} > (C_i/C_{Mn})_{vent}$ or

$(X_i/X_{Mn})_{sed}/(C_i/C_{Mn})_{vent} = E_{Mn}$(ridge sed./vent) > 1

, then the scavenged input from seawater becomes appreciable for element *i*. As shown in Figure 20b, most of the Al, Co, As, Ba, and REE are scavenged from seawater, while most of the B, Mn, Fe, Cu, Zn, Ag, and Pb are supplied mainly by the hydrothermal vents.

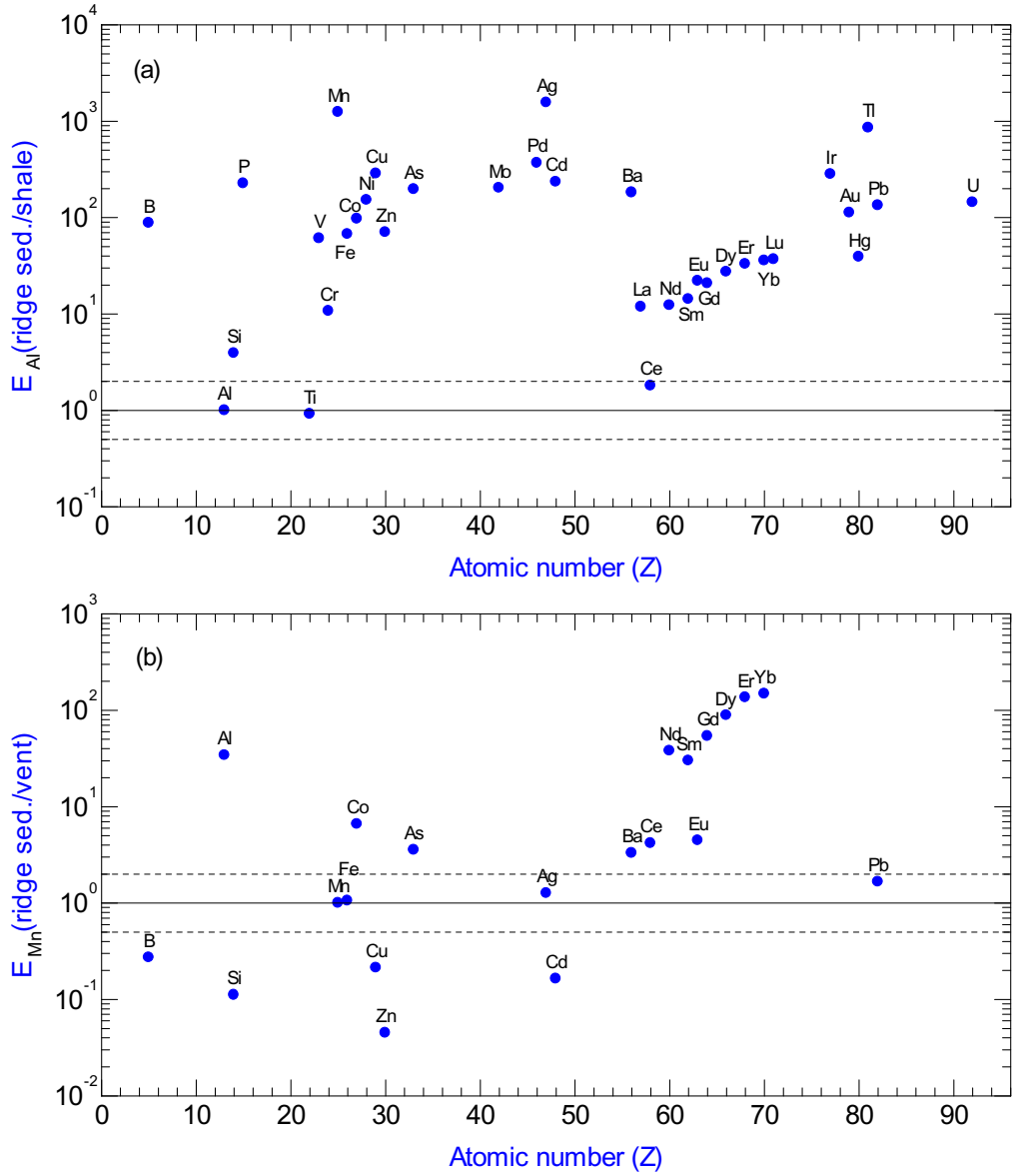

Figure 20: The atomic number versus the enrichment factor (a) E_{Al} (ridge sediment/shale) and (b) E_{Mn}(ridge sediments/vent).

8. Conclusions

The compositions of river water, seawater, hydrothermal vent solutions, river suspended particles, ocean pelagic clay, organisms, and marine manganese nodules do not change randomly. The observed positive correlation between I_z and log X_{sh}/C_R (or log C_R/C_{SW}, log X_{op}/C_{SW}, log X_{org}/C_{SW}, log X_{mn}/C_{SW}, and log X_{MORB}/C_{HY}) for cations, and a negative correlation for anions are consistent with the prediction from the surface complexation model. In other words, the bond strengths between the adsorbed cation and the surface oxygen of hydrated metal oxides, and between the oxygen of adsorbed oxyanion and the surface metal of hydrated metal oxides control the partition of elements between solid and liquid phases in any natural aquatic environment. For Mn, Co, Ce, Pb, and Tl, the oxidative uptake at solid-water interface in the ocean is an additional important process. For alkali and alkaline-earth cations with large ionic radius (such as Cs, Rb, Ba), their relatively small secondary solvation energy further enhances their adsorption onto solid particles.

The inputs of dissolved Mn, Fe, and Zn from the hydrothermal vent solutions may be greater than that from rivers, but a better estimate on the total flux of vent solutions from the mid-oceanic ridge is needed.

Acknowledgement

The Foundation of the Research Institute for Oceanochemistry sponsored this work. Many thanks are due to Professors Yoshiki Sohrin and Shigeru Ohde for their encouragement and support. Discussion with Professor Sohrin was most fruitful. Editorial assistance by Diane Henderson is acknowledged. This work is in part supported by NOAA/OAR/OGP Grant GC02-386. SOEST contribution #7518.

References

Andrews JE, Brimblecombe P, Jiekells TD, Liss PS (1996) *An Introduction to Environmental Chemistry,* Blackwell Science.

Baes CF Jr, Mesmer RE (1976) *The Hydrolysis of Cations*. J. Wiley & Sons.

Balistrieri L, Brewer PG, Murray JW (1981) Scavenging residence times of trace metals and surface chemistry of sinking particles in the deep ocean. Deep Sea Res. 28A, 101–121.

Barth TW (1952) *Theoretical Petrology*. J. Wiley & Sons.

Buffle J (1988) *Compleation Reactions in Aquatic Systems*. Ellis Horwood Limited, England.

Chan LH, Edmond JM, Thompson G, Gillis K (1992) Lithium isotopic composition of submarine basalts: Implications for the lithium cycle in the oceans. Earth Planet. Sci. Lett. 108, 151–160.

Cotton S (1991) *Lanthanides and Actinides,* Oxford University Press.

Firdaus ML, Norisuye K, Nakagawa Y, Nakatsuka S, Sohrin Y (2008) Dissolved and labile particulate Zr, Hf, Nb, Ta, Mo, and W in the western north Pacific Ocean. J of Oceanography 64, 247–257.

Gaillardet J, Viers J, Dupre B (2003) Trace elements in river water, 225–272. In *Water, Weathering, and Soils* (ed.) Vol. 5 *Treatise on Geochemistry* (eds. HD Holland and KK Turekian), Elsevier-Pergamon, Oxford.

Goldberg ED, Arrhenius GOS (1958) Chemistry of Pacific pelagic sediments. Geochim. Cosmochim.

Acta 13, 153–212.
Goldberg S (1985) Chemical modeling of anion competition on goethite using the constant capacitance model. Soil Sci. Soc. Am. J. 49, 851–856.
Goldberg S (1986) Chemical modeling of arsenate adsorption on aluminum and iron oxide minerals. Soil Sci. Soc. Am. J. 50, 1154–1157.
Ishibashi M, Shigematsu T (1951) Chemical studies of the ocean. (XL): On the regularities of the amount of elements dissolved in sea water (2). Bull. Inst. Chem. Res. Kyoto Univ. 27, 42–48.
James RO, Healy TW (1972) Adsorption of hydrolysable metal ions at the oxide-water interface III. A thermodynamic model of adsorption. J. Colloid Interface Sci. 40, 65–81.
Li YH (1981) Ultimate removal mechanisms of elements from the ocean. Geochim. Cosmochim. Acta 45, 1659–1664.
Li YH (1982) A brief discussion on the mean oceanic residence time of elements. Geochim. Cosmochim. Acta 46, 2671–2675.
Li YH (1984) Why are the chemical compositions of living organisms so similar? Schweiz. Z. Hydrol. 4612, 176–184.
Li YH (1991) Distribution patterns of the elements in the ocean: A synthesis. Geochim. Cosmochim. Acta 55, 3223–3240.
Li YH (2000) *A Compendium of Geochemistry: from Solar Nebula to the Human Brain.* Princeton University Press, New Jersey.
Li YH (2006) Are all creatures created equal? (Geochemistry of biosphere). Transactions of the Research Institute of Oceanochemistry 19, 106–112.
Li YH, Burkhardt L, Buchholtz M, O'Hara P, Santschi PH (1984) Partition of radiotracers between suspended particles and seawater. Geochim. Cosmochim. Acta 48, 2011–2019.
Li YH, Schoonmaker J (2003) Chemical composition and mineralogy of marine sediments. in *Sediments, Diagenesis, and Sedimentary Rocks* (ed. F.T. Mackenzie) Vol. 7, *Treatise on Geochemistry* (eds. H.D. Holland and K.K. Turekian), Elsevier-Pergamon, Oxford, 1–35.
Lide DR, chief editor (2001) *CRC Handbook of Chemistry and Physics,* CRC Press, Boca Raton.
Morton JL, Sleep NH (1985) A mid-ocean ridge thermal model: Constraints on the volume of axial hydrothermal heat flux. J. Geophys. Res. 90, 11345–11353.
Schindler PW (1975) Removal of trace metals from the oceans: A zero order model. Thalassia Jugosl. 11,101–111.
Santschi PH, Amdurer M, Adler D, O'Hara P, Li YH, Doering P (1987) Relative mobility of ratioactive trace elements across the sediment-water interface in the MERL model ecosystems of Narragansett Bay. J. Mar. Res. 45, 1007–1048.
Schindler PW, Stumm W (1987) The surface chemistry of oxides, hydroxides, and oxide minerals. In *Aquatic Surface Chemistry,* ed. W Stumm. John-Wiley & Son, New York, 83-110.
Sohrin Y, Fujishima Y, Kazumasa U (1998) Dissolved niobium and tantalum in the North Pacific. Geophys. Res. Lett. 25, 999-1002.
Stumm W, Huang CP, Jenkins SR (1970) Specific chemical interaction affecting the stability of dispersed system. Croat. Chem. Acta 42, 223-245.
Stumm, W. and Morgan, J.J. (1981) *Aquatic Chemistry,* 2nd ed. John Wiley & Son, New York.

Tseng CM, Lamborg C, Fitzgerald WF, Engstrom DR (2004) Cycling of dissolved mercury in Arctic Alaskan lakes. Geochim. Cosmochim. Acta 68, 1173–1184.

Von Damm KL (1995) Controls on the chemistry and temporal variability of seafloor hydrothermal fluids. In *Seafloor Hydrothermal Systems*. eds. Humphris SF, Zierenberg RA, Mullineaux LS, and Thomson RE.

Whitfield M, Turner DR (1987) The role of particles in regulating the composition of seawater. In *Aquatic Surface Chemistry,* ed. W Stumm. John-Wiley & Sons.

Yamamoto T (1983) *Distribution of Trace Element in Marine Algae── Comparative Biological Data.* Kyoto University of Education, Kyoto, Japan.